

Label-free structural characterization of mitomycin C-modulated wound healing after photorefractive keratectomy by the use of multiphoton microscopy

Wen Lo

National Taiwan University
Department of Physics
and
Center of Quantum Science and Engineering
Taipei, 106 Taiwan
and
National Cheng Kung University
Department of Engineering Science
Tainan City, 701 Taiwan

Tsung-Jen Wang

Taipei Medical University Hospital
Department of Ophthalmology
Taipei, 100 Taiwan
and
National Taiwan University Hospital
Department of Ophthalmology
Taipei, 100 Taiwan
and
National Taiwan University College of Medicine
Department of Ophthalmology
Taipei, 100 Taiwan
and
Taipei Medical University
Department of Ophthalmology
Taipei, 100 Taiwan

Wei-Liang Chen

Chiu-Mei Hsueh

National Taiwan University
Department of Physics
and
Center of Quantum Science and Engineering
Taipei, 106 Taiwan

Shean-Jen Chen

National Cheng Kung University
Department of Engineering Science
Tainan City, 701 Taiwan

Yang-Fang Chen

National Taiwan University
Department of Physics
Taipei, 106 Taiwan

Hsiu-Chu Chou

Taipei Medical University
Department of Anatomy
Taipei, 100 Taiwan

Pi-Jung Lin

Universal Eye Center
Taipei, 100 Taiwan

Fung-Rong Hu*

National Taiwan University Hospital
Department of Ophthalmology
Taipei, 100 Taiwan
and
National Taiwan University College of Medicine
Department of Ophthalmology
Taipei, 100 Taiwan

Chen-Yuan Dong*

National Taiwan University
Department of Physics
and
Center of Quantum Science and Engineering
Taipei, 106 Taiwan

Abstract. We applied multiphoton autofluorescence (MAF) and second-harmonic generation (SHG) microscopy to monitor corneal wound healing after photorefractive keratectomy (PRK). Our results show that keratocyte activation can be observed by an increase in its MAF, while SHG imaging of corneal stroma can show the depletion of Bowman's layer after PRK and the reticular collagen deposition in the wound healing stage. Furthermore, quantification of the keratocyte activation and collagen deposition in conjunction with immunohistochemistry and histological images demonstrate the effectiveness of mitomycin C (MMC) in suppressing myofibroblast proliferation and collagen regeneration in the post-PRK wound healing process. © 2010 Society of Photo-Optical Instrumentation Engineers. [DOI: 10.1117/1.3432718]

Keywords: multiphoton autofluorescence excitation; second-harmonic generation; photorefractive keratectomy; collagen; keratocyte activation.

Paper 09348PRR received Aug. 9, 2009; revised manuscript received Mar. 15, 2010; accepted for publication Mar. 16, 2010; published online Jun. 9, 2010.

1 Introduction

Although laser-assisted *in situ* keratomileusis (LASIK) has become increasingly popular for myopia correction, excimer laser-based photorefractive keratectomy (PRK) remains a valuable technique for the highly myopic patient or individual with relatively thin corneas. Nevertheless, the post-PRK wound healing process may lead to the development of corneal haze, resulting in impaired vision.¹ The opacity resulting from the post-operative wound healing process usually devel-

*Address all correspondence to: Chen-Yuan Dong, Department of Physics, National Taiwan University Taipei, Taiwan 106, Taiwan. Tel: 8862-2-3366-5155; Fax: 886-2-2363-9984; E-mail: cydong@phys.ntu.edu.tw or Fung-Rong Hu, National Taiwan University Hospital and College of Medicine, Taipei 100 Taiwan. Tel: 886-2-23123456, ext. 5189; Fax: 886-2-23412875; E-mail: fungronghu@ntu.edu.tw

ops 1 month after the PRK procedure and reaches peak severity 3 months post-surgery. Both epithelial-scraping procedures and PRK have been reported to induce cell apoptosis of keratocytes,^{2,3} with transepithelial PRK inducing less anterior keratocyte apoptosis than laser-scraped PRK.⁴ These results suggest that only the wounds traversing Bowman's layer into the stroma will induce keratocyte activation, where the keratocytes are transformed into spindle-shaped myofibroblasts.^{2,3,5} The transformation of keratocytes into myofibroblasts is characterized by a larger cell appearance, progressive deposition of new extracellular matrix (ECM), and the expression of α smooth muscle actin (α -SMA).^{2,3,5-12} The extent of keratocyte apoptosis and activation also depends on the depth of ablation in the surgery.^{11,13} A possible explanation is that more intensive corneal haze is caused by more severe neural damage from a deeper penetrating wound.¹⁴ It has been proposed that inflammation, epithelial hyperplasia, keratocyte activation, and deposition of new ECM are the factors responsible for increased opacity in post-PRK corneal stroma.¹⁵⁻¹⁷

Recently, mitomycin C (MMC) has been reported as a myofibroblast suppressor to modulate corneal wound healing and prevent corneal haze and regression.¹⁸⁻²⁰ MMC, an alkylating antibiotic derived from *Streptomyces caespitosus*, suppresses the proliferation of rapidly growing cells by inhibiting DNA synthesis.¹⁹ The reports discussing MMC-modulated wound healing usually emphasize keratocyte apoptosis, repopulation, and myofibroblastic transformation. However, the tissue responses after PRK remain to be clarified. For example, the decrease in corneal clarity can result from the different alignment of the regenerated collagen during the wound healing process. These changes in corneal collagen cannot be effectively visualized by standard optical imaging techniques, due to the high transparency of cornea.

In recent years, advances in multiphoton microscopy have rendered label-free imaging of the ocular surface, including the cornea and sclera, a reality.²¹⁻²³ Advantages of this technique include excellent axial-depth penetration and discrimination with significantly reduced photodamage. In this approach, cellular architecture can be visualized by multiphoton autofluorescence (MAF) imaging, while corneal collagen can be imaged using the intrinsic second-harmonic generation (SHG) signal. In this study, we used multiphoton microscopy in conjunction with traditional histology and immunohistology to investigate the wound healing process in rabbit corneas following PRK procedure. To address the potentiality of non-invasively observing myofibroblast formation, we correlate the number of activated keratocytes identified by bright MAF with the number of α -SMA positive myofibroblasts in immunohistochemistry (IHC) imaging. For possible future clinical applications, the SHG signal used to monitor stromal collagen alteration is detected in the backward direction. The effectiveness of post-PRK MMC treatment in suppressing myofibroblast transformation and collagen deposition is also evaluated.

2 Materials and Methods

2.1 Animals and Photorefractive Keratectomy Procedures

The PRK procedures used in this study were approved by the Institute of Animal Care and Use Committee of the College of

Medicine, National Taiwan University. Twelve New Zealand albino rabbits received PRK with 6.5-mm optical zone and 5 diopters correction in both eyes. A flying spot excimer laser (Visx S2, VISX Inc., Santa Clara, California) was used for the PRK procedure. As part of the procedure, each rabbit was anesthetized by intramuscular injection of 2% Rompum (Xylazine) and Zoletil (Tiletamine) at the respective dosages of 0.1 ml and 0.2 ml per kilogram of the rabbit's body mass. In addition, tetracaine eye drops were used for topical anesthesia. To clarify the effectiveness of MMC in modulating post-PRK collagen regeneration, only the left eye of each rabbit was treated with MMC after the PRK procedure. In the MMC treatment, exposed stromal beds were immersed with 0.02% MMC (Kyowa Hakko Kogyo Co., Ltd., Tokyo, Japan) for 30 s and then washed out with phosphate buffered saline (PBS). To obtain time-lapsed features of the tissue regeneration process, the rabbits were sacrificed at day 0 and weeks 1, 2, 4, 8, and 12 after the PRK procedure. The excised rabbit eyeballs were directly placed in a plastic container filled with PBS and mounted on the multiphoton microscope (MPM) for imaging.

2.2 Multiphoton Microscope (MPM)

The home-built multiphoton microscope used in this study has been described previously.²⁴⁻²⁷ Briefly, the output of a mode-locked titanium-sapphire laser (Tsunami, Spectra Physics, Mountain View, California) operating at the wavelength 780 nm was used for excitation. The laser light is reflected by the primary dichroic mirror (700 dcspruv-3p, Chroma Technology, Rockingham, Vermont) and focused by a water-immersion objective (Fluor, 40 \times WI, NA 0.8, Nikon) onto the specimens. A series of beam-controlling optics before the primary dichroic mirror produces circularly polarized excitation at the back aperture of the objective. Due to the polarization dependence of SHG, the use of circularly polarized light allows the production of SHG signal that is independent of collagen fiber direction. The MAF and SHG from the samples were collected by the same objective and separated by a secondary dichroic mirror (435 dcxr, Chroma Technology). The signal is then further filtered by bandpass filters (SHG: HQ390/20, MAF: e435lp-700sp, Chroma Technology), before detection by photomultiplier tubes (R7400P, Hamamatsu, Hamamatsu City, Shizuoka, Japan). The detection bandwidths of the MAF and SHG signals were 435 to 700 nm and 380 to 400 nm, respectively. The use of a broadband autofluorescence filter allows more efficient detection of multiple intrinsic fluorophores inside the keratocytes. Also, in such an epi-configuration setup, the SHG signal is detected in the backward direction. Due to the coherent nature of the SHG process, backward SHG signal can differ from forward SHG signal. Past studies have shown that backward-detected SHG can provide a more global morphology of cornea and has the potential to be applied in the clinical setting.²⁸

For a better understanding of the structural changes and keratocytes distribution within stroma, larger area images were obtained at different depths. A motorized translational stage (H101, Prior Scientific Instruments, Cambridge, UK) was used for specimen translation after each optical scan. In this manner, large-area images 400 by 400 μm^2 in size were acquired in the center of the optical zone. In addition, multi-

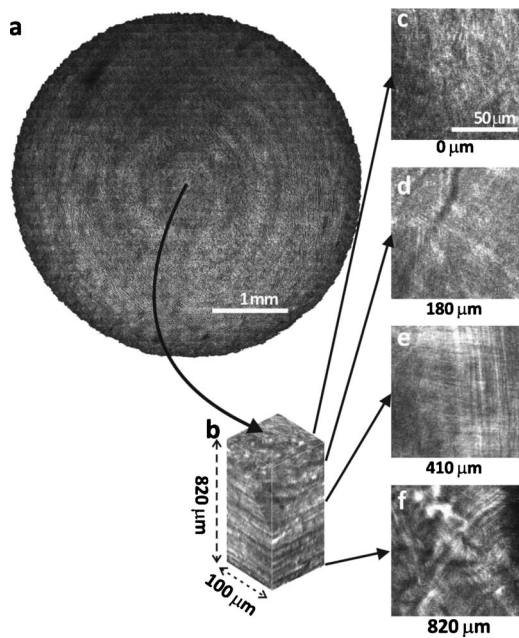


Fig. 1 SHG images of normal rabbit cornea. (a) SHG imaging across entire rabbit cornea. (b) 3-D imaging stack obtained in the central cornea. (c) to (f) *En face* sections in central cornea at the depths of 0, 180, 410, and 820 μm .

photon imaging was performed, at 20- μm steps, throughout the entire cornea thickness. Furthermore, to correct imaging field flatness of the composed large-area images, a customized correction program was used.²⁹

2.3 Histological Preparation

To evaluate the effectiveness of MMC in modulating myofibroblast population, a process related to collagen regeneration, the corneas were fixed in 10% formalin for histological section preparation following multiphoton imaging. Two types of staining were used on adjacent slices. The blue color of Masson's trichrome stain (MTS) was used to identify the collagen in the cornea, while immunohistochemical staining of α -SMA, an expressed protein of myofibroblast, was labeled with diaminobenzidine for its visualization.³⁰

2.4 Quantitative Analysis

To determine the density of myofibroblasts in the anterior stroma, the number of α -SMA positive cells (myofibroblasts) in the immunostained histological sections and the number of activated keratocytes identified by bright MAF in the multiphoton images were separately counted by two investigators of this study. For our purpose, the anterior stroma is defined as the upper 1/3 of the cornea where the keratocytes are concentrated.¹⁰ For calculating the myofibroblast density in the immunohistological section, five nonoverlapped, 100 \times 100 μm^2 regions selected from the anterior region in each cornea were used for cell number counting. Since the immunostained images display a cross-section view of the whole cornea thickness, averaging over the five regions accounts for the density variation due to depth. To correlate activated keratocyte in multiphoton imaging to the myofibroblast number in an immunohistochemical slice, we measured the number of

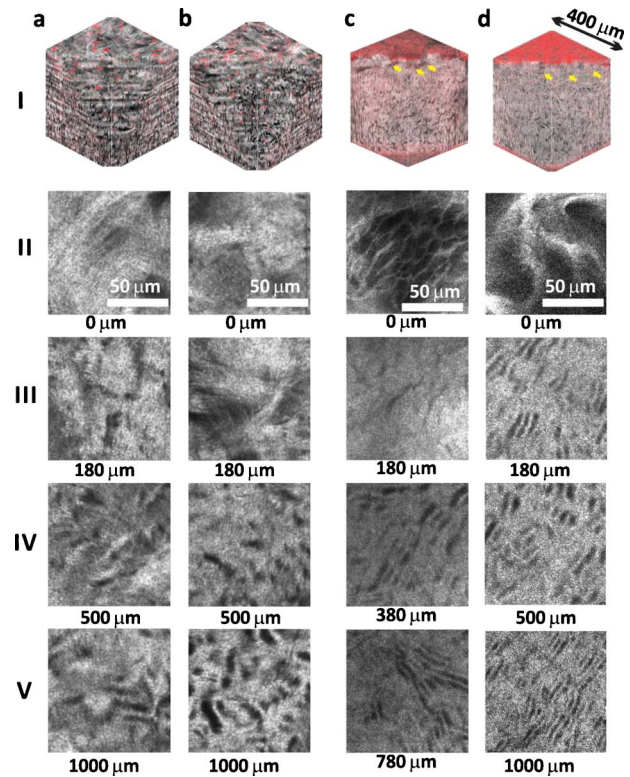


Fig. 2 MAF and SHG imaging of corneas with and without MMC treatment after PRK at day 0 and week 12 [(a) day 0, without MMC; (b) day 0, with MMC; (c) week 12 without MMC; (d) week 12 with MMC] Row I: 3-D reconstructions of the corneas. Rows II to V: *En face* SHG images at stromal surface, depth of 180 μm , middle stroma, and stromal bottom. The red pseudo color and gray scale represent MAF and SHG, respectively. (Color online only.)

MAF positive keratocytes in the *en face* multiphoton images (400 \times 400 μm^2) in the anterior stroma.

Using the SHG images, we can quantify the collagen produced post-PRK procedure. The newly generated collagen can be morphologically identified by its fiber feature in the SHG images. Figure 1 shows the typical fiber morphology at varying depth for a normal rabbit cornea, while in Fig. 2(c) (row II), we see a 12-week post-PRK rabbit cornea displaying newly generated collagen that is morphologically different from that of normal collagen. By calculating the ratio of the thickness of newly regenerated collagen by the full stroma thickness, we obtained the percentage of regenerated collagen in stroma. In the MTS histological sections, new collagen depositions with increased fibrosis appear in dark blue. Measurement of the thickness of the dark blue region can be correlated with the results from the SHG images.

3 Results and Discussion

A large-area backward SHG image across the entire normal rabbit cornea is shown in Fig. 1(a). An image stack and depth-resolved images at the central corneal region are also shown in Figs. 1(b)–1(f). In Fig. 1(a), a global concentric pattern of the stromal collagen can be observed, which agrees with earlier results observed.²⁵ The image stack and the depth-resolved images in Figs. 1(b)–1(f) show that short and interlacing fibers can be observed on the stromal surface, while

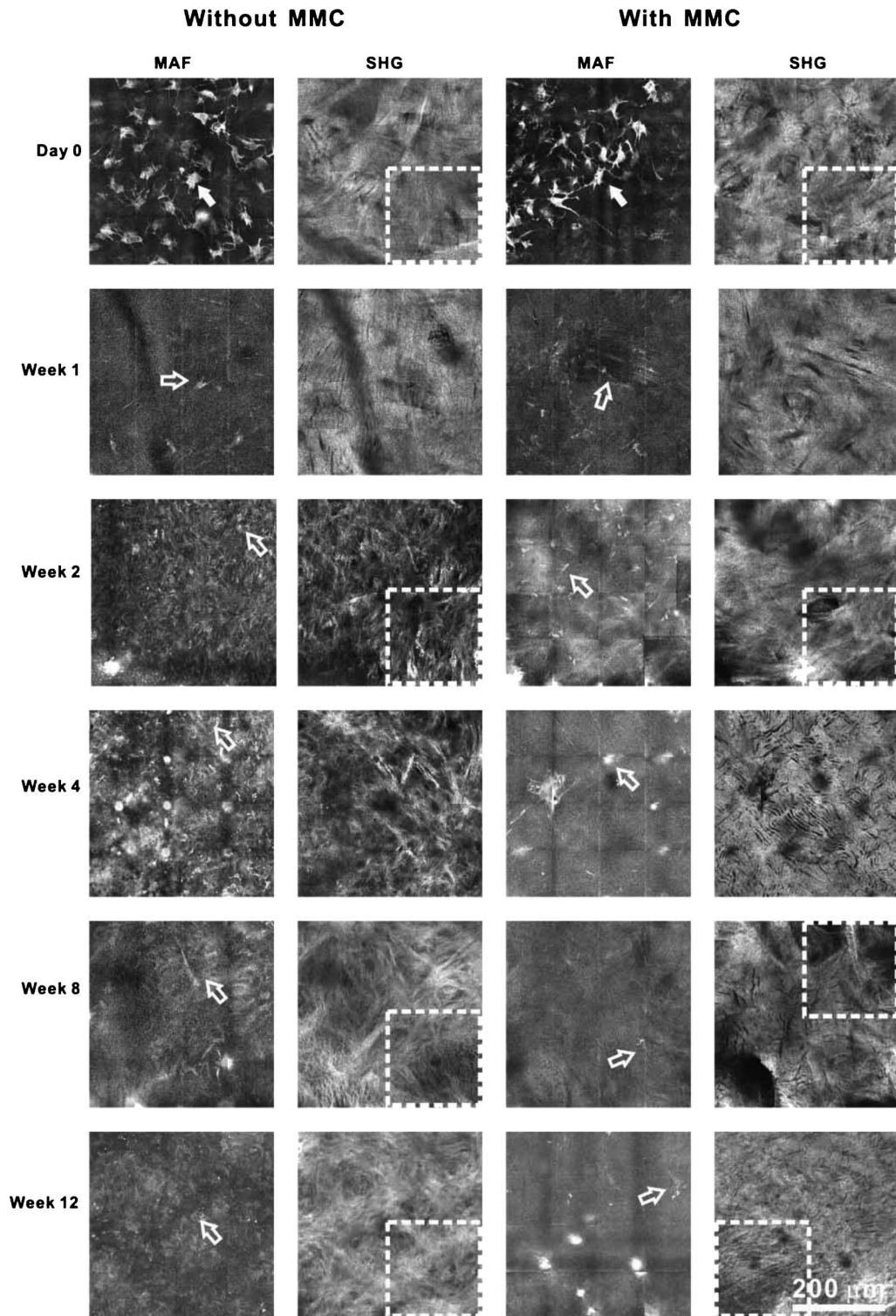


Fig. 3 MAF and SHG images of stromal surface with and without MMC treatment at day 0 and weeks 1, 2, 4, 8, and 12 following PRK procedure. Selected ROIs enclosed by white dashed lines are magnified in Fig. 4. The solid arrows indicate dendritic and activated keratocytes in response to wounding. The open arrows indicate spindle-shaped, activated keratocytes.

global organization of collagen can be imaged in deeper stroma. These observed collagen fiber patterns from rabbit corneas are similar to earlier observation in bovine, porcine, and mice corneas.^{25,26,28}

MAF and SHG imaging of corneas with and without MMC treatment after the PRK procedure at day 0 and week 12 are shown in Fig. 2 [(a): day 0, without MMC; (b): day 0, with MMC; (c): week 12, without MMC; (d): week 12, with

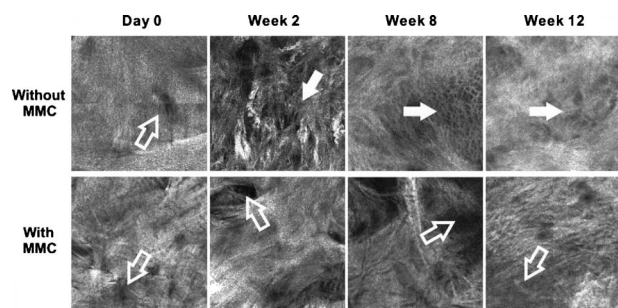


Fig. 4 Magnified SHG images of selected areas in Fig. 3. The solid arrows indicate newly deposited collagen networks. The open arrows point out the unevenness of the stromal surface after PRK treatment.

MMC]. The 3-D reconstructions of corneas are shown in row I of Fig. 2. The MAF and SHG signals are represented by red and gray pseudo-color, respectively. One key feature worthy of notice is that MAF imaging allows the imaging and identification of the epithelium and activated keratocytes. In Figs. 2(a-I) and 2(b-I) MAF positive keratocytes can be observed throughout the full thickness of corneas, with and without MMC treatment. However, in Figs. 2(c-I) and 2(d-I), the MAF positive keratocytes were found to gather in the anterior stroma as the yellow arrows indicated. The SHG images in row II to row V in Fig. 2 demonstrate stromal structure of post-PRK corneas at increasing depths [II: the top stroma ($0\ \mu\text{m}$) or the subepithelial region of cornea; III: at $180\ \mu\text{m}$; IV: the middle stroma; V: the bottom stroma]. In Figs. 2(a-II) and 2(b-II), normal stromal structure of short and interlacing fibers was not found on the top of stroma. At 12 weeks, reticulate, newly generated collagen can be observed in the subepithelial region of corneas without MMC treatment [Fig. 2(c-II)]. The reticulate structure was absent in the week 12 of MMC-treated corneas. However, except for the structural abnormality observed in Fig. 2(d-II), SHG imaging of stroma below $180\ \mu\text{m}$ reveals similar structural morphology as that found in normal corneas. These results suggest that post-PRK wound healing and MMC treatment do not alter the collagen structure in the stroma bed at depth below $180\ \mu\text{m}$.

To focus on the variation at the wounding site, MAF and SHG imaging in the subepithelial region of corneas after different healing times are shown in Fig. 3. Specifically, the difference between post-PRK cornea with and without MMC

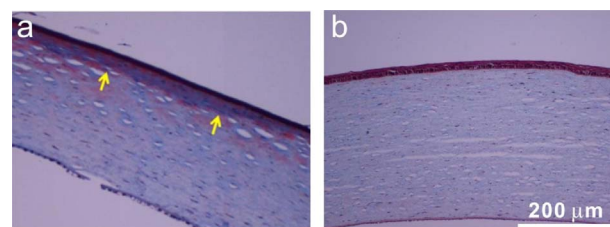


Fig. 5 Masson's trichrome stain of (a) week 12 post-PRK cornea without MMC treatment and (b) normal rabbit cornea without surgery. The dark blue regions, indicated by yellow arrows, are the regions with collagen fibrosis. (Color online only.)

are displayed using MAF and SHG imaging, for day 0 and weeks 1, 2, 4, 8, and 12 post-PRK procedure. Selected regions of interests (ROIs) in the SHG images of Fig. 3 (white dashed squares) are magnified and shown in Fig. 4. Unevenness on the surface is still observed (Fig. 4, open arrows). On the other hand, reticular collagen structure can be observed in corneas without MMC treatment since week 2. Structures of the reticular network, indicated by solid arrows in the magnified images in Fig. 4, suggest that they are the newly deposited collagen. As the healing progressed, the newly generated collagen networks became increasingly dense (Fig. 4; week 12). Moreover, we observe that the stromal bed containing the newly deposited collagen became increasing thick as well. This trend is verified by histological observation (Fig. 5). Figure 5(a) shows the histology with MTS of a post-PRK cornea without MMC treatment, while Fig. 5(b) shows the similarly stained normal cornea without any surgery. The yellow arrows in Fig. 5(a) indicate a dark blue region that is the region with enhanced collagen fibrosis, identified by the reticulate structures of collagen fibers in the SHG images in Fig. 3 and Fig. 4.

To quantify our observation, we measured the ratio of the thickness of newly deposited collagen over the entire stromal bed in both the SHG imaging and MTS histology results (Table 1). The results in Table 1 show that the collagen deposition rate calculated from SHG and MTS imaging is comparable, as both methods show that MMC effectively reduced the collagen deposition after the PRK procedure. Our results show that SHG imaging provides a label-free and less invasive method for measuring the presence of newly deposited collagen than the histological method. In addition, the SHG

Table 1 Percentage of newly generated stroma thickness relative to residual stromal bed. The errors originate from standard deviation of sample means.

	PRK without MMC		PRK with MMC	
	SHG	MTS	SHG	MTS
Week 2	$5.6\% \pm 3.2\%$	Not observed	Not observed	Not observed
Week 4	$8.1\% \pm 1.1\%$	$6.2\% \pm 1.2\%$	Not observed	Not observed
Week 8	$9.0\% \pm 2.1\%$	$8.6\% \pm 1.9\%$	$1.3\% \pm 1.8\%$	$1.40\% \pm 0.5\%$
Week 12	$10.0\% \pm 2.4\%$	$10.9\% \pm 2.4\%$	$2.1\% \pm 0.3\%$	$2.1\% \pm 0.5\%$

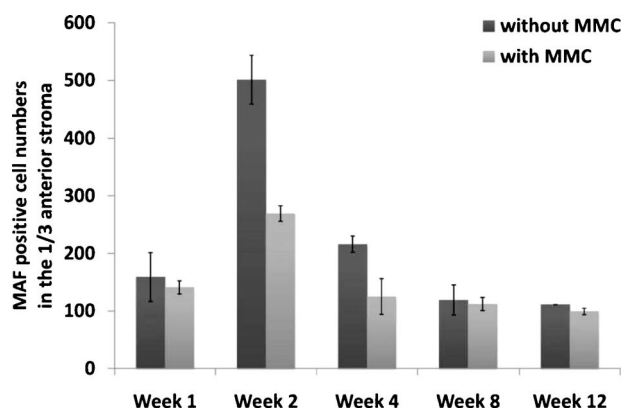


Fig. 6 Temporal analysis of the population of activated keratocytes with detectable MAF.

images and the MAF results in Fig. 3 show the interesting feature of increased level of keratocyte autofluorescence after the PRK procedure. As the solid white arrows in the day 0 MAF images indicate, dendritic keratocyte with bright MAF were observed in corneas both with and without MMC treatment. The increase in keratocyte MAF may be attributed to the elevated level of intracellular metabolism in response to external stress. This effect has been previously reported, and in our case, we can attribute keratocyte MAF activation to the wound healing from the PRK procedure.^{31,32} The open arrows in the MAF images show that keratocytes transformed into spindle-shaped myofibroblasts after week 1.^{33,34} To quantify and correlate our observation with histological results, temporal profiles of keratocyte activation from MAF imaging and α -SMA-positive myofibroblasts from IHC imaging were determined (Fig. 6). Initially, the numbers of MAF-positive, activated keratocytes precipitately increased and peaked at week 2. Then, keratocyte activation subsided after week 4. In addition, the average number of activated keratocytes in the anterior region of corneas without MMC treatment was twice as much as in the MMC-treated corneas at week 2 and week 4. Moreover, the number of activated keratocytes in MMC-treated corneas is always less than that in corneas without the MMC treatment (Fig. 6). In comparison, the temporal profile of IHC-identified myofibroblasts has a very similar trend to the MAF-positive, activated keratocytes (Fig. 7). Our temporal profile of the myofibroblast population is very close to earlier observation in confocal microscopy and immunohistology.^{5,10,13,34,35} These results show that MMC effectively suppressed the appearance of myofibroblasts in IHC images and activated keratocytes in MAF. The observed suppression of the number of myofibroblasts or activated keratocytes by MMC is also consistent with earlier investigations, which showed that MMC reduces the myofibroblast formation rate by increasing cell apoptosis.^{20,35}

We also found that the number of activated keratocytes in MAF is linearly correlated to the number of myofibroblasts in IHC images (Fig. 7). This result suggests that activated keratocytes with detectable MAF in multiphoton imaging can be used to evaluate the amount of myofibroblast related to scar formation and post-PRK corneal haze. The strength of the MAF signal, however, is relatively unaffected by the number of activated keratocytes. A possible explanation is that the

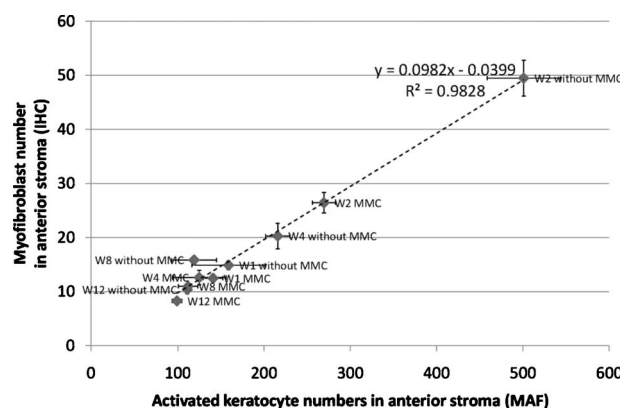


Fig. 7 Correlation between the densities of activated keratocytes in MAF imaging and myofibroblasts in IHC images. R^2 is the linear correlation coefficient.

keratocyte activation process occurs much more quickly than the image acquisition time, so only the maximum MAF signal is observed from the activated keratocytes.

4 Conclusion

In conclusion, we demonstrated that multiphoton microscopy can be used to monitor the alteration in extracellular matrix (ECM) and keratocyte activation in post-PRK corneas. Our results show that MMC decreases the collagen deposition rate during the wound healing process by suppressing the number of myofibroblasts. While similar information relating myofibroblasts and the ECM can be obtained with IHC histology, it is invasive and not suitable for use on a live patient. Clinically friendly reflective confocal microscopy allows the detection of activated keratocytes but cannot be used to monitor the ECM. Since both the SHG and MAF imaging modalities we demonstrated in this work are label-free, our results show that the wound healing process from PRK procedures can be visualized and quantitatively evaluated with minimum invasion.

Acknowledgments

We would like to acknowledge the support of the National Science Council of Taiwan, National Taiwan University Medical College, and Taipei Medical University Hospital Research Grant No. 97TMU-TMUH-10. We also acknowledge the Universal Foundation of Medical Service and Health Care Education, Universal Eye Center, and Mr. Chen-Chih Yao for assisting with the experiment.

References

1. D. K. Williams, "Multizone photorefractive keratectomy for high and very high myopia: long-term results," *J. Cataract Refractive Surg.* **23**(7), 1034–1041 (1997).
2. M. C. Helena, F. Baerveldt, W. J. Kim, and S. E. Wilson, "Keratocyte apoptosis after corneal surgery," *Invest. Ophthalmol. Visual Sci.* **39**(2), 276–283 (1998).
3. R. R. Mohan, A. E. K. Hutcheon, R. Choi, J. W. Hong, J. S. Lee, R. R. Mohan, R. Ambrosio, J. D. Zieske, and S. E. Wilson, "Apoptosis, necrosis, proliferation, and myofibroblast generation in the stroma following LASIK and PRK," *Exp. Eye Res.* **76**(1), 71–87 (2003).
4. W. J. Kim, S. Shah, and S. E. Wilson, "Differences in keratocyte apoptosis following transepithelial and laser-scrape photorefractive keratectomy in rabbits," *J. Refract. Surg.* **14**(5), 526–533 (1998).
5. J. V. Jester, W. M. Petroll, and H. D. Cavanagh, "Corneal stromal

- wound healing in refractive surgery: the role of myofibroblasts," *Prog. Retin Eye Res.* **18**(3), 311–356 (1999).
6. S. K. Masur, H. S. Dewal, T. T. Dinh, I. Erenburg, and S. Petridou, "Myofibroblasts differentiate from fibroblasts when plated at low density," *Proc. Natl. Acad. Sci. U.S.A.* **93**(9), 4219–4223 (1996).
 7. T. Linna and T. Tervo, "Real-time confocal microscopic observations on human corneal nerves and wound healing after excimer laser photorefractive keratectomy," *Curr. Eye Res.* **16**(7), 640–649 (1997).
 8. T. Moller-Pedersen, M. Vogel, H. F. Li, W. M. Petroll, H. D. Cavanagh, and J. V. Jester, "Quantification of stromal thinning, epithelial thickness, and corneal haze after photorefractive keratectomy using *in vivo* confocal microscopy," *Ophthalmology* **104**(3), 360–368 (1997).
 9. T. Moller-Pedersen, H. D. Cavanagh, W. M. Petroll, and J. V. Jester, "Neutralizing antibody to TGF(beta) modulates stromal fibrosis but not regression of photoablative effect following PRK," *Curr. Eye Res.* **17**(7), 736–747 (1998).
 10. T. Moller-Pedersen, H. F. Li, W. M. Petroll, H. D. Cavanagh, and J. V. Jester, "Confocal microscopic characterization of wound repair after photorefractive keratectomy," *Invest. Ophthalmol. Visual Sci.* **39**(3), 487–501 (1998).
 11. T. Moller-Pedersen, H. D. Cavanagh, W. M. Petroll, and J. V. Jester, "Stromal wound healing explains refractive instability and haze development after photorefractive keratectomy—a 1-year confocal microscopic study," *Ophthalmology* **107**(7), 1235–1245 (2000).
 12. J. A. West-Mays and D. J. Dwivedi, "The keratocyte: corneal stromal cell with variable repair phenotypes," *Int. J. Biochem. Cell Biol.* **38**(10), 1625–1631 (2006).
 13. T. Moller-Pedersen, H. D. Cavanagh, W. M. Petroll, and J. V. Jester, "Corneal haze development after PRK is regulated by volume of stromal tissue removal," *Cornea* **17**(6), 627–639 (1998).
 14. T. H. Tuunanen, P. J. Ruusuvaara, R. J. Uusitalo, and T. M. Tervo, "Photoastigmatic keratectomy for correction of astigmatism in corneal grafts," *Cornea* **16**(1), 48–53 (1997).
 15. J. V. Jester, T. Moller-Pedersen, J. Y. Huang, C. M. Sax, W. T. Kays, H. D. Cavanagh, W. M. Petroll, and J. Piatigorsky, "The cellular basis of corneal transparency: evidence for 'corneal crystallins,'" *J. Cell. Sci.* **112**(5), 613–622 (1999).
 16. J. D. Zieske, S. R. Guimaraes, and A. E. K. Hutcheon, "Kinetics of keratocyte proliferation in response to epithelial debridement," *Exp. Eye Res.* **72**(1), 33–39 (2001).
 17. J. C. Varela, M. H. Goldstein, H. V. Baker, and G. S. Schultz, "Microarray analysis of gene expression patterns during healing of rat corneas after excimer laser photorefractive keratectomy," *Invest. Ophthalmol. Visual Sci.* **43**(6), 1772–1782 (2002).
 18. J. H. Talamo, S. Gollamudi, W. R. Green, Z. Delacruz, V. Filatov, and W. J. Stark, "Modulation of corneal wound-healing after excimer laser keratomileusis using topical mitomycin-C and steroids," *Arch. Ophthalmol.* **109**(8), 1141–1146 (1991).
 19. H. Z. Xu, S. Z. Liu, X. B. Xia, P. G. Huang, P. B. Wang, and X. Y. Wu, "Mitomycin C reduces haze formation in rabbits after excimer laser photorefractive keratectomy," *J. Refract. Surg.* **17**(3), 342–349 (2001).
 20. T. I. Kim, H. Tchah, S. A. Lee, K. Sung, B. J. Cho, and M. S. Kook, "Apoptosis in keratocytes caused by mitomycin C," *Invest. Ophthalmol. Visual Sci.* **44**(5), 1912–1917 (2003).
 21. K. Konig, K. Schenke-Layland, I. Riemann, and U. A. Stock, "Multiphoton autofluorescence imaging of intratissue elastic fibers," *Bio-materials* **26**(5), 495–500 (2005).
 22. C. Y. Lin, V. Hovhannisyan, J. T. Wu, C. W. Lin, J. H. Chen, S. J. Lin, and C. Y. Dong, "Label-free imaging of Drosophila larva by multiphoton autofluorescence and second-harmonic generation microscopy," *J. Biomed. Opt.* **13**(5), 050502 (2008).
 23. J. A. Palero, H. S. de Bruijn, A. V. van den Heuvel, H. J. C. M. Sterenborg, H. van Weelden, and H. C. Gerritsen, "*In vivo* nonlinear spectral imaging microscopy of visible and ultraviolet irradiated hairless mouse skin tissues," *Photochem. Photobiol. Sci.* **7**(11), 1422–1425 (2008).
 24. H. Y. Tan, S. W. Teng, W. Lo, W. C. Lin, S. J. Lin, S. H. Jee, and C. Y. Dong, "Characterizing the thermally induced structural changes to intact porcine eye, part 1: second-harmonic generation imaging of cornea stroma," *J. Biomed. Opt.* **10**(5), 054019 (2005).
 25. W. Lo, S. W. Teng, H. Y. Tan, K. H. Kim, H. C. Chen, H. S. Lee, Y. F. Chen, P. T. C. So, and C. Y. Dong, "Intact corneal stroma visualization of GFP mouse revealed by multiphoton imaging," *Microsc. Res. Tech.* **69**(12), 973–975 (2006).
 26. H. Y. Tan, Y. Sun, W. Lo, S. J. Lin, C. H. Hsiao, Y. F. Chen, S. C. M. Huang, W. C. Lin, S. H. Jee, H. S. Yu, and C. Y. Dong, "Multiphoton fluorescence and second-harmonic generation imaging of the structural alterations in keratoconus *ex vivo*," *Invest. Ophthalmol. Visual Sci.* **47**(12), 5251–5259 (2006).
 27. S. W. Teng, H. Y. Tan, J. L. Peng, H. H. Lin, K. H. Kim, W. Lo, Y. Sun, W. C. Lin, S. J. Lin, S. H. Jee, P. T. C. So, and C. Y. Dong, "Multiphoton autofluorescence and second-harmonic generation imaging of the *ex vivo* porcine eye," *Invest. Ophthalmol. Visual Sci.* **47**(3), 1216–1224 (2006).
 28. M. Han, G. Giese, and J. F. Bille, "Second-harmonic generation imaging of collagen fibrils in cornea and sclera," *Opt. Express* **13**(15), 5791–5797 (2005).
 29. V. A. Hovhannisyan, P. J. Su, Y. F. Chen, and C. Y. Dong, "Image heterogeneity correction in large-area, three-dimensional multiphoton microscopy," *Opt. Express* **16**(7), 5107–5117 (2008).
 30. J. D. Bancroft and M. Gamble, *Theory and Practice of Histological Techniques*, Churchill Livingstone/Elsevier, Philadelphia (2008).
 31. D. W. Piston, B. R. Masters, and W. W. Webb, "3-dimensionally resolved Nad(P)H cellular metabolic redox imaging of the *in situ* cornea with 2-photon excitation laser-scanning microscopy," *J. Microsc. (Oxford)* **178**, 20–27 (1995).
 32. A. T. Yeh, N. Nassif, A. Zoumi, and B. J. Tromberg, "Selective corneal imaging using combined second-harmonic generation and two-photon excited fluorescence," *Opt. Lett.* **27**(23), 2082–2084 (2002).
 33. J. V. Jester, W. M. Petroll, P. A. Barry, and H. D. Cavanagh, "Expression of alpha-smooth muscle (Alpha-Sm) actin during corneal stromal wound-healing," *Invest. Ophthalmol. Visual Sci.* **36**(5), 809–819 (1995).
 34. M. E. Fini, "Keratocyte and fibroblast phenotypes in the repairing cornea," *Prog. Retin Eye Res.* **18**(4), 529–551 (1999).
 35. T. I. Kim, J. H. Pak, S. Y. Lee, and H. Tchah, "Mitomycin C-induced reduction of keratocytes and fibroblasts after photorefractive keratectomy," *Invest. Ophthalmol. Visual Sci.* **45**(9), 2978–2984 (2004).